MICROCOPY RESOLUTION TEST CHART

NATIONAL BUREAU OF STANDARDS-1963-A

SPD-807-01

DAVID W. TAYLOR NAVAL SHIP
RESEARCH AND DEVELOPMENT CENTER

Bethesda, Md.   20084

CAVITATION INCEPTION OBSERVATIONS ON
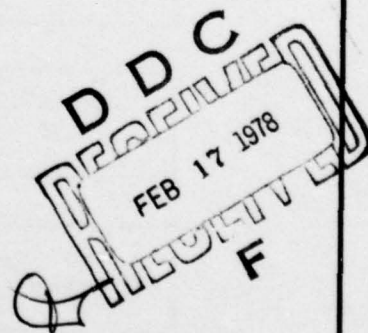TWO AXISYMMETRIC HEADFORMS

by

Thomas T. Huang and Nicholas Santelli

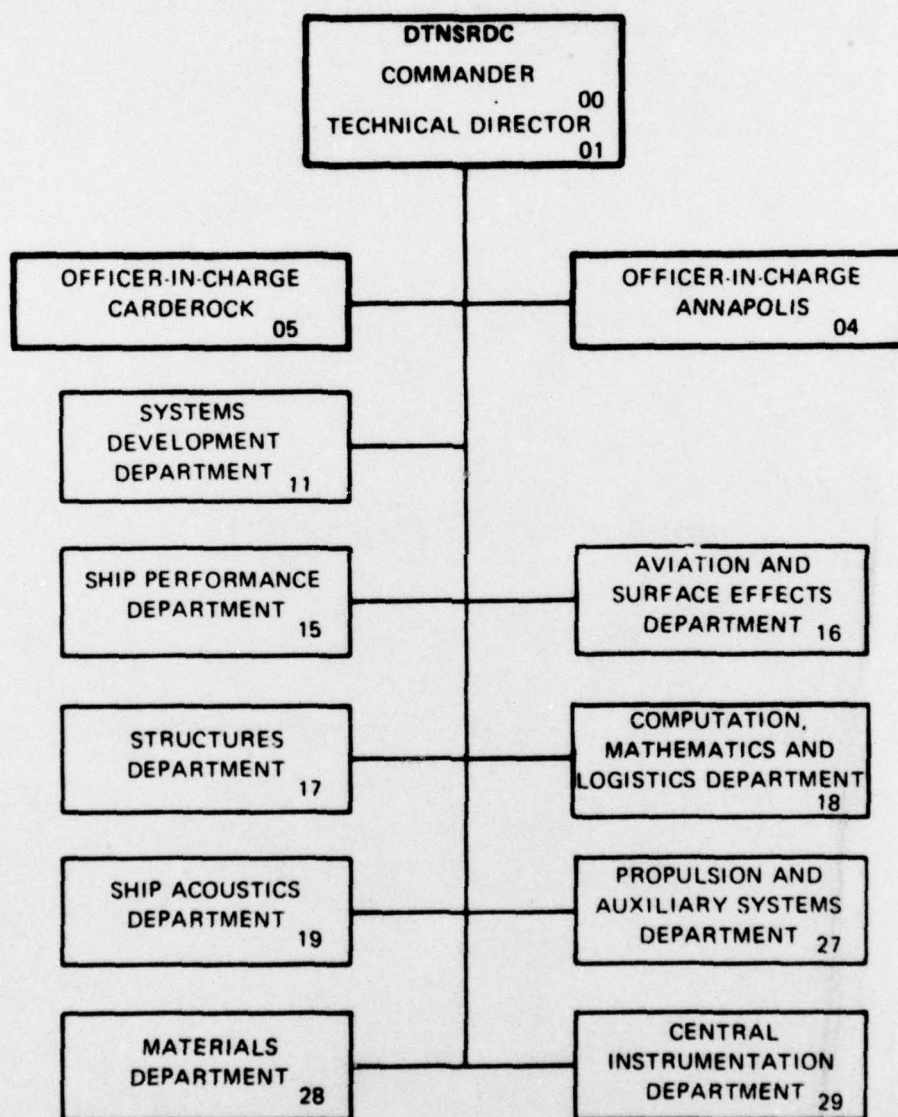APPROVED FOR PUBLIC RELEASE: DISTRIBUTION UNLIMITED

D D C

FEB 17 1978

F

SHIP PERFORMANCE DEPARTMENT
DEPARTMENTAL REPORT

December 1977

SPD-807-01

MAJOR DTNSRDC ORGANIZATIONAL COMPONENTS

SECURITY CLASSIFICATION OF THIS PAGE (When Data Entered)

REPORT DOCUMENTATION PAGE		READ INSTRUCTIONS BEFORE COMPLETING FORM
1. REPORT NUMBER SPD-807-01	2. GOVT ACCESSION NO.	3. RECIPIENT'S CATALOG NUMBER
4. TITLE (and Subtitle) CAVITATION INCEPTION OBSERVATIONS ON TWO AXISYMMETRIC HEADFORMS,		5. TYPE OF REPORT & PERIOD COVERED
		6. PERFORMING ORG. REPORT NUMBER
7. AUTHOR(s) Thomas T. Huang Nicholas Santelli		8. CONTRACT OR GRANT NUMBER(s)
9. PERFORMING ORGANIZATION NAME AND ADDRESS David W. Taylor Naval Ship R&D Center Bethesda, Maryland 20084		10. PROGRAM ELEMENT, PROJECT, TASK AREA & WORK UNIT NUMBERS Task Area 434 52 702 Work Unit 1-1552
11. CONTROLLING OFFICE NAME AND ADDRESS Naval Sea Systems Command (SEA 037) Washington, DC 20362		12. REPORT DATE December 1977
		13. NUMBER OF PAGES 31
14. MONITORING AGENCY NAME & ADDRESS(if different from Controlling Office)		15. SECURITY CLASS. (of this report) UNCLASSIFIED
		15a. DECLASSIFICATION/DOWNGRADING SCHEDULE

16. DISTRIBUTION STATEMENT (of this Report)

APPROVED FOR PUBLIC RELEASE: DISTRIBUTION UNLIMITED

17. DISTRIBUTION STATEMENT (of the abstract entered in Block 20, if different from Report)

SR02381,
F43452

18. SUPPLEMENTARY NOTES

SR0230101,
SF43452702

19. KEY WORDS (Continue on reverse side if necessary and identify by block number)

Cavitation Inception
Viscous Effects
Air Content Effects

20. ABSTRACT (Continue on reverse side if necessary and identify by block number)

Cavitation inception observations on two axisymmetric headforms were made
in the DTNSRDC 36-inch water tunnel. The results indicate that cavitation
inception on a headform with natural flow transition is significantly affected
by the air content of the water. The effect of air content on cavitation
inception on a headform with laminar separation is less pronounced. Visible
cavitation inception never occurred at the locations of minimum static pres-
sure but was observed to occur in the region of natural transition and the

DD FORM
1 JAN 73 1473   EDITION OF 1 NOV 68 IS OBSOLETE
S/N 0102-LF-014-6601   i

UNCLASSIFIED

SECURITY CLASSIFICATION OF THIS PAGE (When Data Entered)

389 694

cont

separated shear layer following laminar separation. It is concluded that both the viscous effects and "cavitatable" microbubble population are extremely important parameters governing the cavitation inception process.

TABLE OF CONTENTS

LIST OF FIGURES

LIST OF TABLES

ABSTRACT

Cavitation inception observations on two axisymmetric headforms were made in the DTNSRDC 36-inch water tunnel. The results indicate that cavitation inception on a headform with natural flow transition is significantly affected by the air content of the water. The effect of air content on cavitation inception on a headform with laminar separation is less pronounced. Visible cavitation inception never occurred at the locations of minimum static pressure but was obs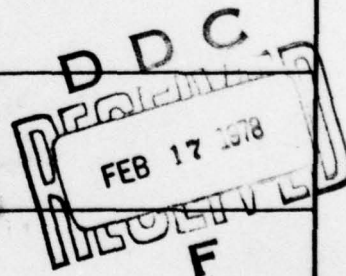erved to occur in the region of natural transition and the separated shear layer following laminar separation. It is concluded that both the viscous effects and "cavitatable" microbubble population are extremely important parameters governing the cavitation inception process.

ADMINISTRATIVE INFORMATION

INTRODUCTION

Inception of cavitation in liquid is the condition under which cavitation is first detected, either visually or acoustically with a simple measuring device. The simple assumption that equilibrium conditions are reached instantaneously and that the cavitation inception occurs immediately when the static pressure on the body is equal to the vapor pressure, has often been made in most engineering predictions of cavitation inception. However, physically, a finite length of time is required for the vaporization and a finite amount of work has to be done against the surface-tension forces. Therefore, for cavitation inception to take place, the element of

liquid has to remain for some finite time in a region where the pressure
is equal to or less than the vapor pressure. The required residence time
is controlled by the concentration and size distribution of critical
"cavitatable" nuclei (weak spots) from which cavitation actually grow
explosively, and by the viscous characteristics of the flow regime (whether
laminar, laminar-separated, transitional, or fully-turbulent) through which
the element of liquid has to pass, for cavitation inception to take
place.

Cavitation inception on the ITTC (International Towing Tank Con-
ference) standard headform was found[1] to appear in many different physical
forms when tested in different cavitation facilities around the world.
Cavitation inception on this single headform occurred over the range of
cavitation numbers from 0.4 to 1.1. The follow-up study by Johnsson[2] and
the review by Acosta and Parkin[3] suggested that in some cases inception
appeared in the form of an attached band (ring) cavity as the result of
laminar separation and in other cases, inception appeared in the form of
traveling macroscopic bubbles as a result of natural flow transition
which precluded laminar separation. It is known that a laminar boundary
layer on a smooth body is quite stable from the forward stagnation point
up to the location of $C_{p_{min}}$. Further downstream the flow may or may not
separate depending upon the magnitude of the adverse pressure gradient.
For a body having laminar separation, Arakeri and Acosta[4,5] designated

1. Lindgren, H. and C.A. Johnsson, "Cavitation Inception on Head Forms,
    ITTC Comparative Experiments," Proceedings 11th International Towing
    Tank Conference, Tokyo, pp. 219-232 (1966).

2. Johnsson, C.A., "Cavitation Inception on Head Forms, Further Tests,"
    Proceedings 12th International Towing Tank Conference, Rome,
    pp. 381-392 (1969).

3. Acosta, A.J. and B.R. Parkin, "Cavitation Inception- A Selective
    Review," Journal of Ship Research, Vol. 19, No. 4, pp. 193-205
    (1975).

4. Arakeri, V.H. and A.J. Acosta, "Viscous Effects in the Inception of
    Cavitation on Axisymmetric Bodies," Journal of Fluids Engineering,
    ASME, Vol. 95, Series 1, No. 4, pp. 519-528 (1974).

5. Arakeri, V.H. and A.J. Acosta, "Cavitation Inception Observations on
    Axisymmetric Bodies at Supercritical Reynolds Numbers," Journal of
    Ship Research, Vol. 20, No. 1, pp. 40-50 (1976).

the Reynolds number at which laminar separation disappeared as the critical Reynolds number, $R_{D_{crit}}$. Flows for which the Reynolds number respectively is less than or more than $R_{D_{crit}}$ are called "subcritical" and "supercritical." For supercritical Reynolds numbers and for bodies without the possibility of laminar separation, there is some evidence[4,5] that cavitation inception takes place within the region of transition from laminar to turbulent flow. For subcritical Reynolds numbers, cavitation inception is found to occur in the transition region of the separated shear layer or in the reattachment region following laminar separation.[4,5] Enormous pressure fluctuations on the body surface were measured by Arakeri[6] and Huang and Hannan[7] in the reattachment region following laminar separation. In addition, amplitudes of the pressure fluctuations in the natural transition region measured by Huang and Hannan[7] were found to be higher than in a fully-turbulent boundary-layer flow by a factor ranging from 2 to 3. Cavitation inception[4,5] is believed to be closely related to the high pressure fluctuations in the region following laminar separation and in the natural transition zone of an attached boundary layer. The transition process is very sensitive to the magnitude of the free-stream turbulence level and the surface condition of the body. Thus, the location of cavitation-prone transition regions and the critical Reynolds number may be different for the same body in two different facilities or, for that matter, it may be different in the same facility if the free-stream turbulence level or the surface roughness is changed. The effect of surface roughness on cavitation inception, although extremely important, falls outside the scope of the present investigation.

The growth of critical microscopic bubbles (weak spots) into the ultimately visible macroscopic cavitation in the cavitation-prone transition region depends not only upon the nature of the transition process, the presence or the absence of laminar separation, but also upon the population of the critical bubbles either within the flow or on the liquid solid interface. Some cavitation facilities are equipped with deaeration

---

6   Arakeri, V.H., "A Note on the Transition Observation on an Axisymmetric Body and Some Related Fluctuating Wall Pressure Measurements," Journal of Fluids Engineering, ASME, Vol. 97, Series 1, No. 1, pp. 82-87 (1975).

7   Huang, T.T. and D.E. Hannan, "Pressure Fluctuations in the Regions of Flow Transition," DTNSRDC Report 4723 (1975).

and/or resorber systems, but others have none at all. Therefore, the concentration of critical microbubbles may vary significantly from one facility to the other so as to cause the large discrepancies between observed cavitation inception indices for the ITTC headform. The actual size range of the critical microbubbles from which cavitation grows explosively is still not known. Peterson[8] has holographically measured the particle size distribution of free microbubbles with radii varying from 25 to 200 microns in the 12-inch water tunnel. The number of microbubbles in this size range was found to be reduced significantly if the total measured dissolved gas content of the water referred to test section pressure, α/α_{TS}, was reduced to a value smaller than 0.9. The cavitation inception indices measured by Peterson[8] and Brockett[9] on a modified ellipsoidal headform (known as the NSRDC headform[3,5] with $C_{p_{min}}$ = -0.84) showed that the cavitation inception index decreased with decreasing air content at supercritical Reynolds numbers.

The effect of gross air content on cavitation inception was first reported by Crump[10,11]. Significant effects of air content on cavitation inception on hydrofoils was reported by Layne[12] and on model propeller was

8   Peterson, F.B., "Hydrodynamic Cavitation and Some Considerations of
     the Influence of Free-Gas Content," 9th Symposium on Naval Hydro-
     dynamics, Paris, (Aug 1972); Available in U.S. Government Printing
     Office, ACR-203, Vol. 2, pp. 1131-1186 (1972).

9   Brockett, T., "Some Environmental Effects on Headform Cavitation
     Inception," NSRDC Report 3974 (1972).

10   Crump, S.F., "Critical Pressures for the Inception of Cavitation in
     a Large-Scale Numachi Nozzle as Influenced by the Air Content of
     the Water," DTMB Report 770 (1951).

11   Crump, S.F., "Determination of Critical Pressures for the Inception
     of Cavitation in Fresh and Sea Water as Influenced by Air Content
     of Water," DTMB Report 575 (1949).

12   Layne, D.B., "Inception Cavitation Results on 16-012 and 16-(0.15)12
     Hydrofoils in 24- and 36-Inch Water Tunnels," NSRDC Report 4578
     (1975).

4

noted by Weitendorf.[13] Viscous effects on cavitation inception were examined thoroughly by Arakeri and Acosta.[4,5] However, in order to fully understand the cavitation inception process, both the nuclei population and viscous effects should be considered together.

Recently Gates[14] found that air content and free-stream turbulence level had a dramatic effect on cavitation inception on the NSRDC headform, but had negligible effect on a hemispheric nose. The critical Reynolds number $R_{D_{crit}}$ of the NSRDC headform measured by Schlieren photographs[5,10] in the CIT high-speed water tunnel was between 3.3×10^5 to 5×10^5 with a turbulence level at about 0.25 percent. In the CIT-low-turbulence water tunnel, $R_{D_{crit}}$ decreased from about 5×10^5 at a turbulence level of 0.04 percent to about 1.6×10^5 for a turbulence level of 3.8 percent. The critical Reynolds number of the same NSRDC headform measured from fluorescent oil paint in the DTNSRDC 12-inch water tunnel[9] was 1.6×10^5 at a turbulence level[15] of about 2 percent. On the other hand, the critical Reynolds number of the hemispheric nose was above the speed capability of the CIT high-speed water tunnel[4] and was estimated by using the spatial amplification method to be higher than 5×10^6. The Gates[14] data show that cavitation inception on a body having a low value of critical Reynolds number seems to be more susceptible to the effects of freestream turbulence level and the population of the critical microbubbles. Thus, cavitation

---

13   Weitendorf, E.A., "Cavitation and Its Influence on Induced Hull Pressure Amplitudes," Presented at Symposium on Hydrodynamics of Ship and Offshore Propulsion Systems, Høvik outside Oslo, Norway, sponsored by Det Norske Veritas (Mar 1977).

14   Gates, E.M., "The Influence of Freestream Turbulence, Freestream Nuclei Populations and a Drag-Reducing Polymer on Cavitation Inception on Two Axisymmetric Bodies," CIT Report No. Eng. 183-2 (1977).

15   Blake, W.K., et al, "Effect of Boundary-Layer Development on Cavitation Noise and Inception on a Hydrofoil," DTNSRDC 76-0051 (1976).

inception on a body with natural transition, where the critical Reynolds number may be regarded as zero, may be expected to be very sensitive to variations in nuclei population and free-stream turbulence level. The interaction between viscous effects and the population of the free micro-bubbles is not fully understood.

Huang and Peterson[16] evaluated the influence of viscous effects on the correlation of model and full-scale cavitation inception. Large discrepancies between model and full-scale cavitation inception number were noted when the pressure fluctuations in the region of natural transition or laminar separation were superimposed upon the static pressure. The locations of the cavitation-prone transition regions were shown to move closer to the points of minimum static pressure as Reynolds number was increased from model to full-scale.

In order to gain further insight into the physics of cavitation inception and its effect on model/full-scale cavitation-inception correlation, two axisymmetric headforms were tested in the DTNSRDC 36-inch water tunnel. Detailed measurements of wall-pressure fluctuations in the transitions regions were made previously by Huang and Hannan.[7] Visible cavitation inception never occurred at the locations of minimum static pressure but was observed in the regions of natural transition and following laminar separation. The present results indicate that the observed cavitation inception on the headform with natural transition is significantly affected by the air content of the water. The effect of the air content on cavitation inception on the headform with laminar separation is less pronounced.

GEOMETRY AND FLOW FOR TWO AXISYMMETRIC HEADFORMS

The two axisymmetric headforms selected for this cavitation-inception investigation were chosen because detailed measurements of wall-pressure fluctuations during natural flow transition and following laminar separation had been previously made on them by Huang and Hannan.[7] One of the headforms,

---

16 Huang, T.T. and F.B. Peterson, "Influence of Viscous Effects on Model Full-Scale Cavitation Scaling," Journal of Ship Research, Vol. 20, No. 4, pp. 215-223 (1976).

6

designated "T-3", has a natural transition region without any possibility
of laminar separation. The other headform, designated "S-2", exhibits laminar
separation. Each headform was connected by a portion of parallel middle body
to a propeller shaft housing located on the downstream side of the closed
jet test section of the Center's 36-inch water tunnel. The head-
form entrance-length-to-diameter ratios, L_E/D, are 1.82 and 1.00, respectively.
The offsets of the two headforms are described in terms of Granville's[17]
family of polynomials by the expression

$$\eta^2 = 0.8333 R(\varsigma) + 10 K(\varsigma) + Q(\varsigma) \tag{1}$$

where
$$R(\varsigma) = 2\varsigma(\varsigma-1)^4$$
$$K(\varsigma) = \frac{1}{3}\varsigma^2(\varsigma-1)^3$$
$$Q(\varsigma) = 1 - (\varsigma-1)^4(4\varsigma+1)$$
$$\varsigma = x/L_E$$
$$\eta = 2y/D$$

Here, x is the axial distance from the nose and y is the local body radius.
This particular choice made for coefficients insures that the slopes and
curvatures of the headforms are continuous along their entire length,
including points of intersection with the parallel middle body, $x = L_E$. The
diameter, D, of Headform T-3 is 9.84 cm (3.875 inches) and 7.63 cm
(3 inches) for Headform S-2. The headforms were constructed of
aluminum, and were polished to a 0.81 micron (32 micro-inch) finish. They
were carefully anodized to avoid corrosion in water, and to maintain the same
surface finish.

The body contour, distribution of potential-flow pressure coefficients
$C_p = (p-p_o)/(\rho U_o^2/2)$, computed amplification ratios of boundary-layer
disturbances, and the measured flow regimes on Headform T-3 in the Center's
Anechoic Flow Facility are shown in Figure 1. The minimum pressure coefficient

---

17   Granville, P.S., "Geometrical Characteristics of Noses and Tails for
     Parallel Middle Bodies," NSRDC Report 3763 (1972).

$C_{p_{min}}$ is -0.187 and is located at x/D = 1.10. The cumulative spatial amplification ratio A as a function of distance along the body surface was computed from a step-by-step integration starting from the neutral stability point by a computer code (DABL)[18] for a band of discrete critical dimensionless frequencies. The computed locations for the most rapidly growing disturbances reaching $A = e^N$ for N = 0, 3, 5, 7, 9, 11, and 13 are shown in Figure 1. The flow regimes measures by Huang and Hannan[7] in the Center's Anechoic wind tunnel are also plotted in Figure 1. The free-stream turbulence levels $\overline{u'}^2 / U_o$ were less than 0.1 percent in the R_D range of the wind tunnel experiments, where $R_D = U_o D / \nu$, U_o is the free-stream velocity, D, is the diameter of the headform, and ν is the kinematic viscosity of the fluid. However, the free-stream turbulence level measured by a hot-film anenometer at the centerline of the water tunnel was 0.5 percent for velocities under 15 meter/sec and was about 1 percent for velocities above 15 meter/sec due to low-frequency oscillations of the water tunnel. The measured transition locations on Headform T-3 in the wind tunnel correlated quite well with the computed locations of $A = e^{11}$. The free-stream turbulence level in the water tunnel is higher than that in the wind tunnel. Therefore, transition on Headform T-3 in the water tunnel is expected to occur at locations where A is less than e^{11}. The wall-pressure fluctuations in the transition region at four values of R_D were measured by Huang and Hannan[7] and the results are shown in Figure 2. The root-mean-square amplitude of the wall-pressure fluctuations increases rapidly in the bursting regime starting at the location of $A = e^{11}$, reaches a maximum value at the location where $A = e^{13}$, and gradually approaches the amplitude of pressure fluctuations for a fully-turbulent flow. The maximum rms wall-pressure fluctuation measured in the transition region was found to be about $0.04 \rho U_o^2/2$ with a negative pressure-peak fluctuation, at about $0.2 \rho U_o^2/2$. The frequently occurring large negative pressure fluctuation $-p'_{minc}$ should be superimposed upon the static pressure

18   von Kerczek, C. and N.C. Groves, "Disturbance Amplification in
      Boundary Layers," DTNSRDC Report to be published in December 1977.

8

in the natural transition region for the estimation of cavitation inception. The condition under which cavitation events occur about once every second is a criterion often used for cavitation inception.[9] This criterion is used here to determine the value of $-p'_{minc}$. Using the results of Huang and Hannan[7], the value of $-p_{minc}$ was found to be about $0.1 \rho U_o^2/2$ by Huang and Peterson.[16] This value may be reduced somewhat in the water tunnel due to the high level of free-stream turbulence.

The body contour and the distribution of C_p on Headform S-2 are shown in Figure 3. The minimum pressure coefficient $C_{p_{min}}$ is -0.405 and is located at $x/D = 0.68$. Laminar separation is predicted by the Curle-Skan modified-Thwaites criterion,[19] $(\theta_s^2/\nu)(dU/dS) \leq -0.09$ for separation, to occur at $x/D = 0.89$, where θ_s is the momentum thickness at separation and dU/dS is the velocity gradient along the body surface. Use of fluorescent oil-film visualization verified the existence of laminar separation at $x/D = 0.89$. The calculated spatial amplification ratios at the predicted separation point, A_s, shown in Figure 4, are less than e^7 for the range of Reynolds numbers, $R_D \leq 1.3 \times 10^6$, used in the water tunnel. The appearance of attached band cavitation starting at the separation point of Headform S-2 implies the existence of laminar separation (see Results). In the Anechoic wind tunnel where free-stream turbulence levels are low, the observed transition locations on Headform T-3 were found to occur at about $A = e^{11}$, and laminar separation was found to occur on Headform S-2 up to $R_D = 2.44 \times 10^6$. At this R_D the amplification ratio at the separation point is e^{11} (Figure 4). The appearance of laminar separation on Headform S-2 in the water tunnel at $A = e^7$ for $R_D = 1.3 \times 10^6$ leads one to conclude that the transition locations on Headform T-3 and the critical Reynolds numbers on Headform S-2 in the water tunnel are correctly predicted to fall within the range of $e^7 < A < e^{11}$. Henceforth, we use a value of $A = e^9$, with the uncertainty range of $e^7 < A < e^{11}$, to estimate transition locations for the present water tunnel data.

---

19 Curle, N. and S.W. Skan, "Approximate Methods for Predicting Separation Properties of Laminar Boundary Layers," Aeronautical Quarterly, Vol. 8, pp. 257-268 (1957).

According to Gaster,[20] the Tollmien-Schlichting disturbances grow
rapidly in the shear layer above a laminar separation bubble. The flow
becomes turbulent a short distance downstream of the bubble, and the increase
of mixing due to the turbulent motion causes the separation flow to reattach.
In the vicinity of reattachment, violent turbulent motions take place, and
the boundary layer establishes fully turbulent flow characteristics a
very short distance downstream of flow reattachment. The computed values
of $R_{\theta_s} = \theta_s U_s / \nu$, and measured values of ξ / θ_s, and λ / θ_s at
the separation point, determined by fluorescent oil-film visualization and
hot-film probes,[7] are shown in Figure 4, where λ is the length of the separa-
tion bubbles; ξ is the length between the separation point and reattachment
point, where the pressure fluctuation has its highest value[7]; θ_s is
the momentum thickness at the separation point; and U_s is the local potential
flow velocity at the separation point. As shown in Figure 5, the maximum
rms wall-pressure fluctuations in the reattachment region are found to be
$\sqrt{\overline{p'^2}} = 0.15 \, \rho \, U_0^2 / 2$ and the minimum negative pressure peaks, $-p'_{min}$, are
about $0.55 \ U_0^2/2$. The large negative pressure fluctuations, p'_{minc}, which
occur once per second and may trigger cavitation inception, are about
$-0.35 \ U_0^2/2$. The static pressure underneath a separation bubble was found by
Gaster[20] to deviate slightly from the potential-flow pressure distribution
if the separation bubble was short, i.e., if $R_{\theta_s} > 150$ for Headform S-2;
there was little deviation in static pressure due to flow separation after
reattachment. On the basis of Gaster's criteria[20] the laminar separation
bubbles on Headform S-2 in the water tunnel were all short bubbles since
$R_{\theta_s} > 500$ for the range of R_D investigated here (Figure 5).

EXPERIMENTAL TECHNIQUES

Cavitation measurements for the two axisymmetric headforms have been
carried out in the David W. Taylor Naval Ship Research and Development

20 Gaster, M., "The Structure and Behavior of Laminar Separation Bubbles,
    Separated Flows," Advisory Group for Aerospace Research and
    Development Conference Proceedings 4, Part 2, pp. 813-854 (1966).

Center (DTNSRDC) 36-inch variable-pressure water tunnel with a closed-jet test section. The pressure in the test section can be varied between 1.38×10^5 and 4.14×10^6 dynes/cm^2 (2 and 60 pounds/inch^2) absolute. A cylindrical resorber 7.62 metres in diameter and 21.3 metres in height is built into the circuit to permit more efficient control of the free-air content of the water. The tunnel is also equipped with a deaeration system which can be used to reduce the air content of the water. Total air content was measured by a standard Van Slyke apparatus, and the water temperature in the test section was also sensed by a thermocouple and was displayed by a Honeywell-Brown "Electronik" precision indicator. The speed of the tunnel was determined from the pressure difference between two points along the contraction sections, upstream of the test section. This pressure difference and the pressure at the centerline of the test section were measured by differential gages and were displayed digitally on the tunnel control panel.

The headform was attached to the housing of the propeller shaft located at the centerline of the test section and was illuminated by a EG&G Xenon stroboscope (Model LS148). This system allowed the visual observation of cavitation bubbles. Cavitation inception was also independently measured by an accelerometer mounted on the inside wall of the headform. It was found that the output of the accelerometer registered the collapse of each cavitation bubble. The accelerometer output correlated well with the visual observation of cavitation under the stroboscopic lighting condition. Cavitation inception is arbitrarily defined in this report as the onset of detectable cavitation events which occur about once a second. Most of the cavitation events on the two headforms were recorded photographically by using Polaroid high-speed Type-52 film or Kodak high-speed Ektachrome 32-mm film, exposed under a 25-microsecond light pulse of the tunnel stroboscopic system. In addition, high-speed motion pictures were taken by a Red Lake Hycam 16-mm camera with a 120-metre film capacity. The lighting for the high-speed motion pictures was provided by three Sylvania Type-3 flash bulbs with a pulse duration of 20 milliseconds. At each exposure, the instantaneous tunnel speed and pressure were recorded from the digital output of the pressure gages. This

practice was used to reduce the error in computing cavitation number due to the undesired low-frequency tunnel oscillation at speeds above 15 metres/sec.

Incipient cavitation numbers were determined by slowly lowering the tunnel pressure at constant tunnel velocity until cavitation events occurred about once every second. Desinent cavitation numbers were determined by increasing the tunnel static pressure and noting the disappearance of cavitation. In all cases, the cavitation numbers will be characterized by

$$\sigma = \frac{p_o - p_v}{\frac{1}{2}\rho U_o^2} \tag{2}$$

where p_v is the vapor pressure of the water, p_o is the static pressure at the centerline of the test section, and U_o is the tunnel velocity. The incipient cavitation numbers are denoted by σ_i and the desinent cavitation number by σ_d.

Cavitation observations were made with dissolved air contents on the order of 9 and 18 ppmw (parts per million by weight), corresponding to 40 and 80 percent of saturation at $21^\circ C$ water temperature and atmospheric pressure. No quantitative measurements of free-gas bubble distribution were made in the present experiment. However, the microbubbles in the test section were plentiful and should have been proportional to the measured dissolved gas content of the water referred to test section pressure,[8] α/α_{TS}.

CAVITATION CHARACTERISTICS OF HEADFORM T-3 WITH NATURAL TRANSITION

Based on the previous wind tunnel experiments, natural transition without any possibility of laminar separation was expected in the water tunnel for Headform T-3. As shown in Figure 2, the large pressure fluctuations measured on Headform T-3 in the low free-stream turbulence wind tunnel occur in the region where $e^{12} < A < e^{14}$. For a relatively high free-stream turbulence level, the actual transition can only be

12

estimated to occur in the region of $1.56 < x/D < 1.72$ corresponding to the region where $e^7 < A < e^{11}$ at the highest Reynolds number tested in the water tunnel (Figure 1). The location where $A = e^9$ at $R_D = 1.68 \times 10^6$ is $X/D = 1.65$.

A large number of high-speed photographs were taken under stroboscopic light with a pulse duration of 25 microseconds. Figure 6 shows stroboscopic photographs of various stages of cavitation on Headform T-3 at $R_D = 1.68 \times 10^6$. At a 9-ppmw air content, only a few visible traveling expanding cavitation bubbles could be detected at the lowest limit of the tunnel pressure capability ($\sigma = 0.135$). Therefore, no further reduction of air content was attempted. The desinent cavitation number σ_d at a 9-ppmw air content is taken to be 0.135. Cavitation events at $\sigma = 0.135$ occur at a rate less than one occurrence per second.

At high air content of 18 ppmw ($\alpha / \alpha_S = 0.80$), under which the water in the test section was super-saturated with air, various cavitation events on Headform T-3 were observed. As shown in Figure 6a, the beginning of discrete visible traveling and growing cavitation bubbles in the region $1.4 < x/D < 1.7$ was detected at $\sigma = 0.173$. The average size of the visible bubbles was estimated to be on the order of 500 microns. By careful visual observation and by examining the high-speed motion pictures, it was found that the explosive cavitation bubbles did not originate from the macrobubbles of 500 microns or larger. The exact sizes of the cavitable free microbubbles were not measured in the present investigation.

Upon further lowering of the tunnel pressure at constant tunnel velocity, the occurrence of growing cavitation bubbles became more frequent (Figure 6b). The occurrence of visible cavitation bubbles at a rate of once every second was defined as incipient cavitation. The incipient cavitation number of Headform T-3 was determined to be 0.17 ± 0.005 at 18 ppmw air content and $R_D = 1.68 \times 10^6$. However, at a 9-ppmw air content, the incipient cavitation number was determined to be smaller than 0.135. The visible expanding cavitation bubbles were detected in the region of $1.4 < x/D < 1.7$ which approximated the estimated transition

region of Headform T-3 in the water tunnel at $R_D = 1.68 \times 10^6$.

It may be noted that the actual growth process of the critical microbubbles must take place at some distance upstream of the transition region, presumably starting at the location where the local pressure first reaches vapor pressure. This growth process may be slow in the laminar flow region where bubble residence times are longer although not verified, it may be possible for cavitation to occur upstream of the transition region of a large laminar body which has provided sufficiently long bubble residence time. Once bubbles are in the vicinity of the transition region, the turbulence bursting process with its large pressure fluctuations enhances the rate of bubble growth. The explosive growth of microbubbles into visible cavitation bubbles is controlled by the pressure fluctuations and the supply of free microbubbles which can interact with the turbulence bursting process.

As shown in Figures 6c and 6d, the collapse of cavitation bubbles on the body in the region $1.7 < x/D < 2.2$ became visible with further reduction of cavitation number. Occasionally spot cavitation was observed, presumably because slight imperfections of the surface finish became nucleation sources. Intensive cavitation with large collapsing macro-bubbles (1000-3000 microns) and/or large spot cavitation in the region $1.5 < x/D < 2.5$ were observed at $\sigma = 0.14$ (Figure 6e). The tunnel pressure was then increased slowly and the condition under which no cavitation bubbles were visible was defined as desinent cavitation. The value of σ_d for Headform T-3 was found to be 0.18 ± 0.005 which was very close to the value of $-C_{p_{min}}$ (0.187). The difference between σ_d and σ_i is also very small.

As shown in Table 1, the local static pressure coefficients at the locations of $A = e^9$ and e^{11} ($x/D = 1.65$ and 1.72) at $R_D = 1.68 \times 10^6$ are -0.115 and -0.100, respectively. We assume that[14] cavitation inception occurs when the superposition of the local static pressure in the transition region and the large negative pressure fluctuations reaches a pressure equal to or less than vapor pressure, i.e.,

14

$$\sigma_i = -C_{ptr} - C_{pt} \tag{3}$$

where σ_i is the incipient cavitation number, C_{ptr} is the static pressure coefficient in the transition region, and $-C_{pt}$ is the negative pressure fluctuation coefficient to be superimposed on the static pressure coefficient ($-C_{pt} = -p'_{minc}/(1/2\rho U_o^2)$). The measured value of σ_i and σ_d on Headform T-3 at an 18-ppmw air content were 0.17 and 0.18, respectively. However, the measured values of σ_i and σ_d at a 9-ppmw air content were both less than 0.135. As shown in Table 1, the value of C_{pt} can be experimentally deduced from the measured value of σ_i or σ_d and the computed value of C_{ptr}. As shown in Table 1, the difference in the deduced values of C_{pt} at two different air contents implies that there is significant interaction between the viscous effects and the critical microbubbles population. This interaction warrants detailed investigation.

CAVITATION CHARACTERISTICS OF HEADFORM S-3 WITH LAMINAR SEPARATION

Recall from Figures 3 and 4 that Headform S-2 has laminar separation at $x/D = 0.89$, the value of $C_{p_{min}}$ is -0.405 at $x/D = 0.68$, and at $R_D = 1.3 \times 10^6$ the computed amplification ratio at the separation point, A_s, is e^7. This relatively high amplification ratio at the separation point indicates that transition from laminar to turbulent flow is about to take place there. Once laminar separation occurs, the separated shear layer will rapidly become turbulent a short distance further downstream. The increasing mixing due to the turbulence causes the separated shear layer to reattach. The location of the maximum wall-pressure fluctuations measured in the low-turbulence wind tunnel[7] is $\xi / \theta_s = 330$ (Figure 4). The axial location of the maximum wall-pressure fluctuation is $(x/D)_s + (\xi/D)_s = 0.89 + (\xi/\theta_s)(R_{\theta_s}/R_D)(U_o/U_s) = 1.03$. The local potential-flow pressure coefficients at the separation point and at the location of maximum measured wall-pressure fluctuations in the reattachment region are respectively -0.30 and -0.15.

At a cavitation number σ of 0.30 ± 0.01, attached cavitation fingers similar to those shown in Figure 7a appear and disappear

15

randomly. Occasionally, macrobubbles of the order of 500 ~ 1000 microns
are visible in the reattachment region at x/D = 1.0 $\overset{+}{-}$ 0.05. Cavitation
fingers occur more frequently with further lowering of the cavitation
number to 0.26 (see Figure 7a). At σ = 0.245 $\overset{+}{-}$ 0.01 the cavitation
fingers merge together to form a ring cavity (Figure 7b). The leading
edge of the ring is located at about x/D = 0.90 which is a short distance
downstream of the laminar separation point. The desinent cavitation
number was determined to be 0.31 $\overset{+}{-}$ 0.01, which is very close to the value
of the incipient cavitation number. No cavitation was observed at the
point of the minimum potential-flow static pressure at x/D = 0.68. It
is also very interesting to note that there was no noticeable difference
in cavitation characteristics of Headform S-2 at the two air contents of
9 and 18 ppmw. The parameters controlling cavitation inception on Head-
forms S-2, the ITTC and NSRDC headforms, and a hemispheric nose are listed in
Table 2 for further reference.

<div align="center">DISCUSSION AND CONCLUSIONS</div>

Cavitation inception on two axisymmetric headforms did not
occur at the locations of minimum static pressure but was observed to
occur further downstream at the locations of natural flow transition on
Headform T-3 or following laminar separation on Headform S-2.

Cavitation in the natural transition region on Headform T-3 was
usually characterized by traveling bubbles. On the basis of the present
results for Headform T-3 and the results of Arakeri and Acosta[4] for a
1.5 calibre ogive, the incipient or desinent cavitation number of a
body with natural transition may be determined by superimposing an
unsteady pressure coefficient C_{pt} upon the local potential-flow static
pressure coefficient, C_{ptr} at the transition location, i.e.,

$$\left(\begin{matrix} \sigma_i \\ \sigma_d \end{matrix} \right) = -C_{ptr} - C_{pt} \tag{4}$$

The present results for Headform T-3 suggest that the value of $-C_{pt}$ is
about 0.06 for incipient cavitation and about 0.07 for desinent cavitation

at 18 ppmw air content; at 9 ppmw the value of $-C_{pt}$ is about 0.03 for desinent cavitation and is smaller than 0.03 for incipient cavitation. For a 1.5 calibre ogive at 10 ppmw air content, the value of $-C_{pt}$ is about 0.02 for desinent cavitation.[4] At supercritical Reynolds numbers, Brockett[9] reported the traveling-bubble type of cavitation inception on the NSRDC headform and found that the value of σ_i increases with increasing values of R_D at a given air content and with increasing air content ranging from 0.2 to 11 ppmw at a given value of R_D. Although the location of transition and thus the values of $-C_{ptr}$ in the Brockett[9] experiments are not known, the trend of increasing σ_i with increasing R_D is consistent with Equation (4). The dependence of σ_i, and hence C_{pt} on air content is also consistent with the present results. The above results suggest that traveling bubble-type cavitation will occur at the natural transition region and that the incipient or desinent cavitation number depends upon the distribution of microscopic cavitation bubbles available in the water. The interaction of the viscous effects and the critical microbubble population warrants further investigation.

The present results for Headform S-2 show that cavitation fingers suddenly occur a short distance from the separation point when the cavitation number is about equal to $-C_{ps}$, the negative of the potential-flow pressure coefficient at the separation location. This finger-type cavitation near the separation point was also reported on the ITTC head-forms[1,2,3,4,5] and on the NSRDC headform[3,5] at high subcritical values of Reynolds number. When the subcritical Reynolds number approaches the critical Reynolds number, the separated shear layer will become more susceptible to disturbances and finger-type cavitation will usually occur at $\sigma_i \approx -C_{ps}$. Further decrease of σ will eventually lead to the formation of a single attached ring cavity around the headform. The parameters controlling cavitation inception on these three headforms and a hemispheric nose are listed in Table 2.

On the other hand, the cavitation inception observed by Arakeri and Acosta[4,5] on a hemispheric nose was very different in appearance.

17

The Reynolds numbers in their experiments were one order of magnitude smaller than the critical Reynolds number, so that the separated shear layer was less susceptible to disturbances. Generally, the finger-type cavitation did not occur near the separation point at low subcritical values of Reynolds numbers. The macroscopic bubbles were first observed in the reattachment region, presumably starting at the flow transition point of the separated shear layer, about 130-180 θ_s from the separation point.[16] A further reduction in cavitation number produced increasing mounts of macroscopic cavitation bubbles, and eventually resulted in the formation of a single attached ring cavity. Under this condition, the incipient cavitation index can be approximated by

$$\sigma_i = - C_{ptr} - C_{pt}$$

The location of transition in the separated shear layer was measured by Arakeri and Acosta[4] with a Schlieren visualization technique. By using the potential-flow value of C_{ptr} at the measured transition location[4] and the measured value of σ_i , the value of $-C_{pt}$ is deduced to be 0.45 ± 0.05 which is compatible with the large negative pressure fluctuations which have been measured in a reattachment region.[7] The separated shear layer immediately following laminar separation is not very susceptible to disturbances and cavitation inception in the transition region in a shear layer, at large distances downstream of the separation point (130 θ_s - 180 θ_s), is related to the resulting enormous pressure fluctuations. The observations of Gates[14] have shown that incipient cavitation on a hemispheric nose is insensitive to changes in the nuclei population distribution and the free-stream turbulence level.

Cavitation inception on Headform S-2 with laminar separation was found to be unaffected by a change of air content from 9 ppmw to 18 ppmw. However, Gates observed dramatic effects of the air content and the free-stream turbulence level on cavitation inception on the NSRDC headform.[14] At inception, both the S-2 headform and the NSRDC headform had finger-type cavitation near separation, but the NSRDC headform at R_D = (1.5 to 4.2) x 10^5 is more sensitive to the effect of air content than Head-

18

form S-2 at $R_D = 1.3 \times 10^6$. Further investigation is necessary to
clarify this discrepancy. A clear description of the flow character-
istics associated with finger-type cavitation near laminar separation is
required.

ACKNOWLEDGMENT

REFERENCES

1. Lindgren, H. and C.A. Johnsson, "Cavitation Inception on Head Forms, ITTC Comparative Experiments," Proceedings 11th International Towing Tank Conference, Tokyo, pp. 219-232 (1966).

2. Johnsson, C.A., "Cavitation Inception on Head Forms, Further Tests," Proceedings 12th International Towing Tank Conference, Rome, pp. 381-392 (1969).

3. Acosta, A.J. and B.R. Parkin, "Cavitation Inception - A Selective Review," Journal of Ship Research, Vol. 19, No. 4, pp. 193-205 (1975).

4. Arakeri, V.H. and A.J. Acosta, "Viscous Effects in the Inception of Cavitation on Axisymmetric Bodies," Journal of Fluids Engineering, ASME, Vol. 95, Series 1, No. 4, pp. 519-528 (1974).

5. Arakeri, V.H. and A.J. Acosta, "Cavitation Inception Observations on Axisymmetric Bodies at Supercritical Reynolds Numbers," Journal of Ship Research, Vol. 20, No. 1, pp. 40-50 (1976).

6. Arakeri, V.H., "A Note on the Transition Observation on an Axisymmetric Body and Some Related Fluctuating Wall Pressure Measurements," Journal of Fluids Engineering, ASME, Vol. 97, Series 1, No. 1, pp. 82-87 (1975).

7. Huang, T.T. and D.E. Hannan, "Pressure Fluctuations in the Regions of Flow Transition," DTNSRDC Report 4723 (1975).

8. Peterson, F.B., "Hydrodynamic Cavitation and Some Considerations of the Influence of Free-Gas Content," 9th Symposium on Naval Hydrodynamics, Paris, (August 1972); Available in U.S. Government Printing Office, ACR-203, Vol. 2, pp. 1131-1186 (1972).

9. Brockett, T., "Some Environmental Effects on Headform Cavitation Inception," NSRDC Report 3974 (1972).

10. Crump, S.F., "Critical Pressures for the Inception of Cavitation in a Large-Scale Numachi Nozzle as Influenced by the Air Content of the Water," DTMB Report 770 (1951).

11. Crump, S.F., "Determination of Critical Pressures for the Inception of Cavitation in Fresh and Sea Water as Influenced by Air Content of Water," DTMB Report 575 (1949).

12. Layne, D.E., "Inception Cavitation Results on 16-012 and 16-(0.15) 12 Hydrofoils in 24- and 36-Inch Water Tunnels," NSRDC Report 4578 (1975).

13. Weitendorf, E.A., "Cavitation and Its Influence on Induced Hull Pressure Amplitudes," Presented at *Symposium on Hydrodynamics of Ship and Offshore Propulsion Systems*, Høvik outside Oslo, Norway, sponsored by Det Norske Veritas (Mar 1977).

14. Gates, E.M., "The Influence of Freestream Turbulence, Freestream Nuclei Populations and a Drag-Reducing Polymer on Cavitation Inception on Two Axisymmetric Bodies," CIT Report No. Eng. 183-2 (1977).

15. Blake, W.K., et al, "Effect of Boundary-Layer Development on Cavitation Noise and Inception on a Hydrofoil," DTNSRDC Report 76-0051 (1976).

16. Huang, T.T. and F.B. Peterson, "Influence of Viscous Effects on Model Full-Scale Cavitation Scaling," *Journal of Ship Research*, Vol. 20, No. 4, pp. 215-223 (1976).

17. Granville, P.S., "Geometrical Characteristics of Noses and Tails for Parallel Middle Bodies," NSRDC Report 3763 (1972).

18. von Kerczek, C. and N.C. Groves, "Disturbance Amplification in Boundary Layers," DTNSRDC Report

19. Curle, N. and S.W. Skan, "Approximate Methods for Predicting Separation Properties of Laminar Boundary Layers," *Aeronautical Quarterly*, Vol. 8, pp. 257-268 (1957).

20. Gaster, M., "The Structure and Behavior of Laminar Separation Bubbles, Separated Flows," Advisory Group for Aerospace Research and Development Conference Proceedings 4, Part 2, pp. 813-854 (1966).

Table 1

Experimentally Deducted Values of Pressure Fluctuation Coefficient
in the Transition Region which Cause Incipient and Desinent
Cavitation at Two Air Contents

A	e^7	e^9	e^{11}	Average value of the deducted $-C_{pt}$ in the region of e^9 A e^{11}
$\dfrac{x}{D}$	1.56	1.65	1.72	
$-C_{p_{tr}}$	0.135	0.115	0.10	
18 ppmw air content $\;\sigma_i = 0.17$	0.035	0.055	0.07	0.063
18 ppmw air content $\;\sigma_d = 0.18$	0.045	0.065	0.08	0.073
9 ppmw air content $\;\sigma_d = 0.135$	0	0.020	0.035	0.028

Deducted $-C_{p_t} = \sigma_i - (-C_{p_{tr}})$

Table 2

Parameters Controlling Cavitation Inception on Headforms
with Laminar Separation

|		Hemispheric Nose	Headform S-2	ITTC Headform	NSRDC Headform
References		4, 5, 14	7, Present	1,2,3,4,5	3,5,8,9,14
Predicted[18] $R_{D_{crit}} \times 10^6$ by	e^7	5.0	1.3	1.3	0.42
	e^9	7.0	1.9	2.1	0.64
	e^{11}	9.0	2.5	3.0	0.86
Measured $R_{D_{crit}} \times 10^6$		>0.9(CIT HSWT[4]) >2.5(DTNSRDC[7])	>1.3 (present) >2.4 (DTNSRDC[7])	>0.88(CIT HSWT[4])	≈0.5 (CIT HSWT[5]) ≈0.5 (CIT LTWT[14]) ≈0.16(DTNSRDC[9])
$-C_{P_{min}}$		0.78	0.405	0.59	0.84
(x/D) at $C_{P_{min}}$		0.39	0.68	0.30	0.03
$-C_{P_s}$		0.63	0.30	0.45	0.40
$(x/D)_s$		0.47	0.89	0.465	0.435
$(S/D)_s$		0.76	1.10	0.82	0.83
Measured σ_i		$\sigma_i = 0.75+0.05$ at $R_D \approx (5 \times 10^5)$ $\sigma_i = 0.875+0.03$ at $R_D \approx 9 \times 10^5$	$\sigma_i = 0.30$ at $R_D = 1.3 \times 10^6$	$\sigma_i = 0.46$ at $R_D = 8.8 \times 10^5$	$\sigma_i = 0.44+0.04$ at $R_D = (3\ 4) \times 10^5$
σ_i versus $-C_{P_s}$		$\sigma_i \neq -C_{P_s}$ $\sigma_i = -C_{ptr}+0.45$	$\sigma_i = -C_{P_s}$	$\sigma_i = -C_{P_s}$	$\sigma_i = -C_{P_s}$
Incipient Cavitation Type for $R_{D\ crit}$		Bubbles Ring	Fingers Ring	Fingers Ring	Fingers Ring
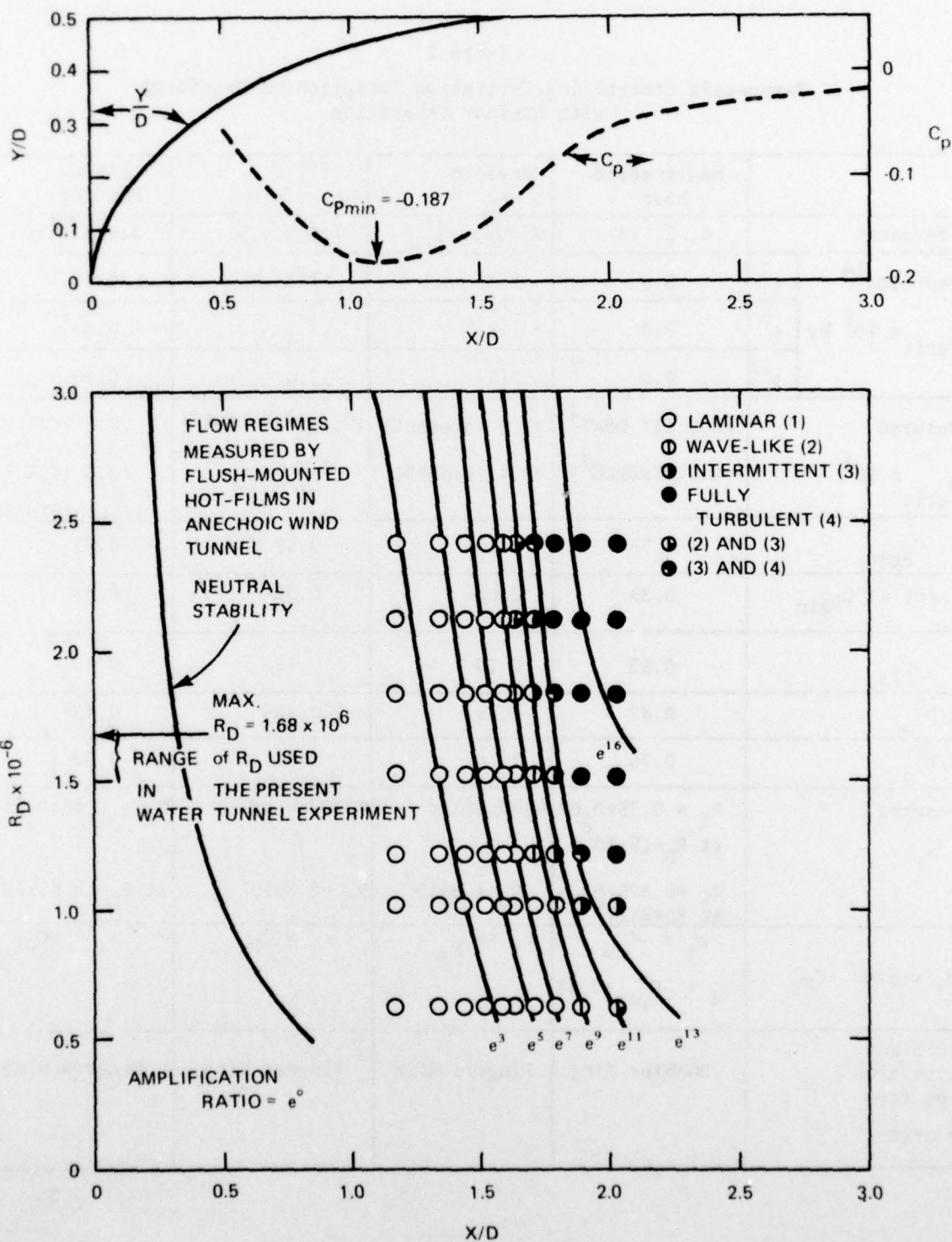
Figure 1 – Surface Profile, Pressure Coefficients, Amplification Ratios, and Measured Flow Regimes on Headform T-3
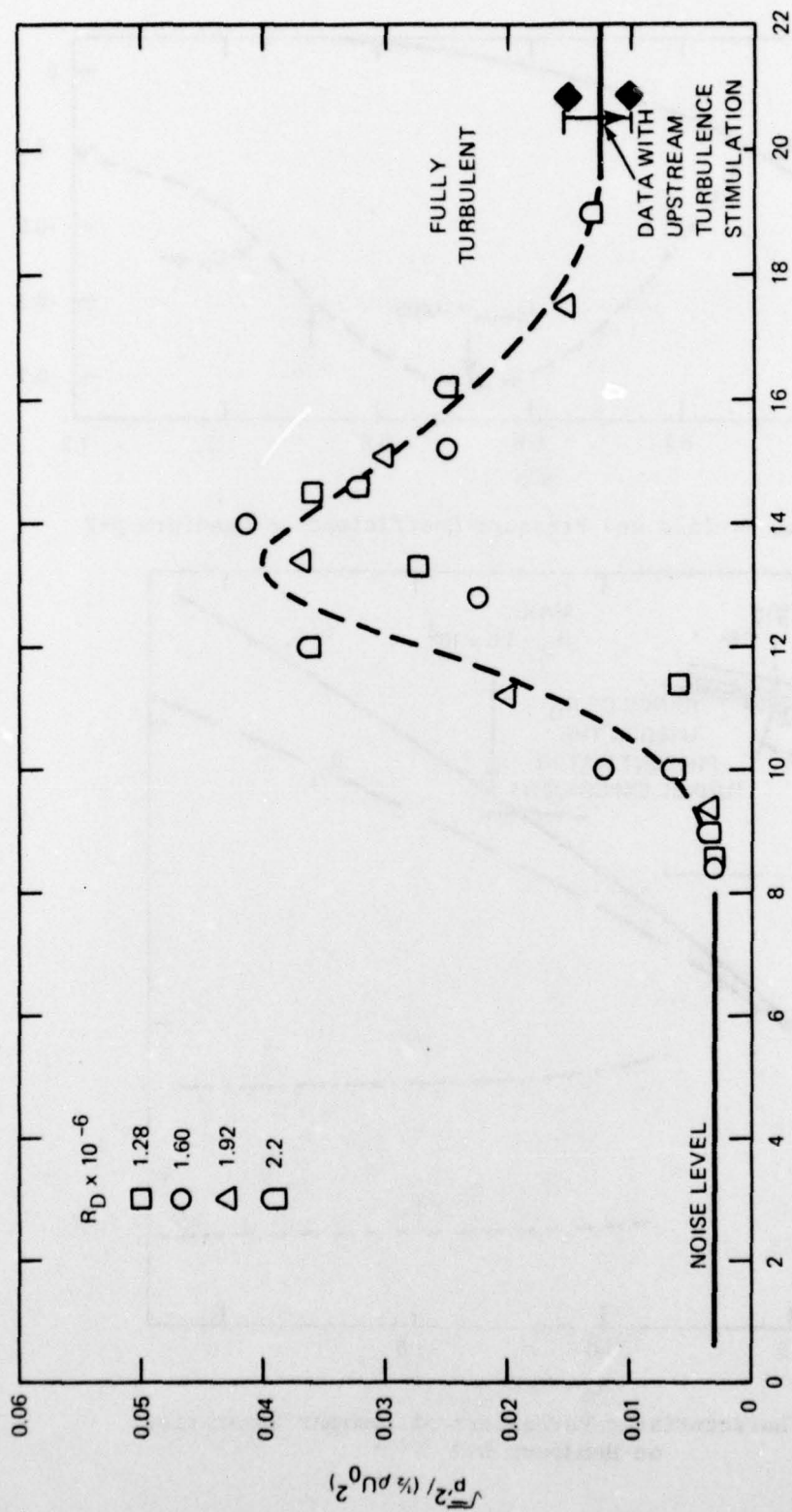
Figure 2 – Root-Mean-Square Wall Pressure Fluctuation In The Natural
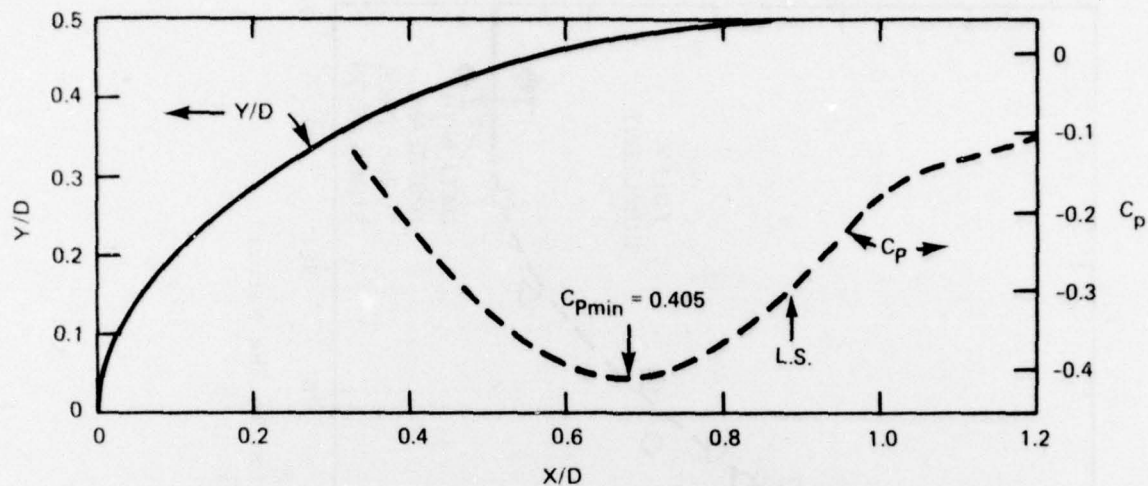Transition Region of Headform T-3

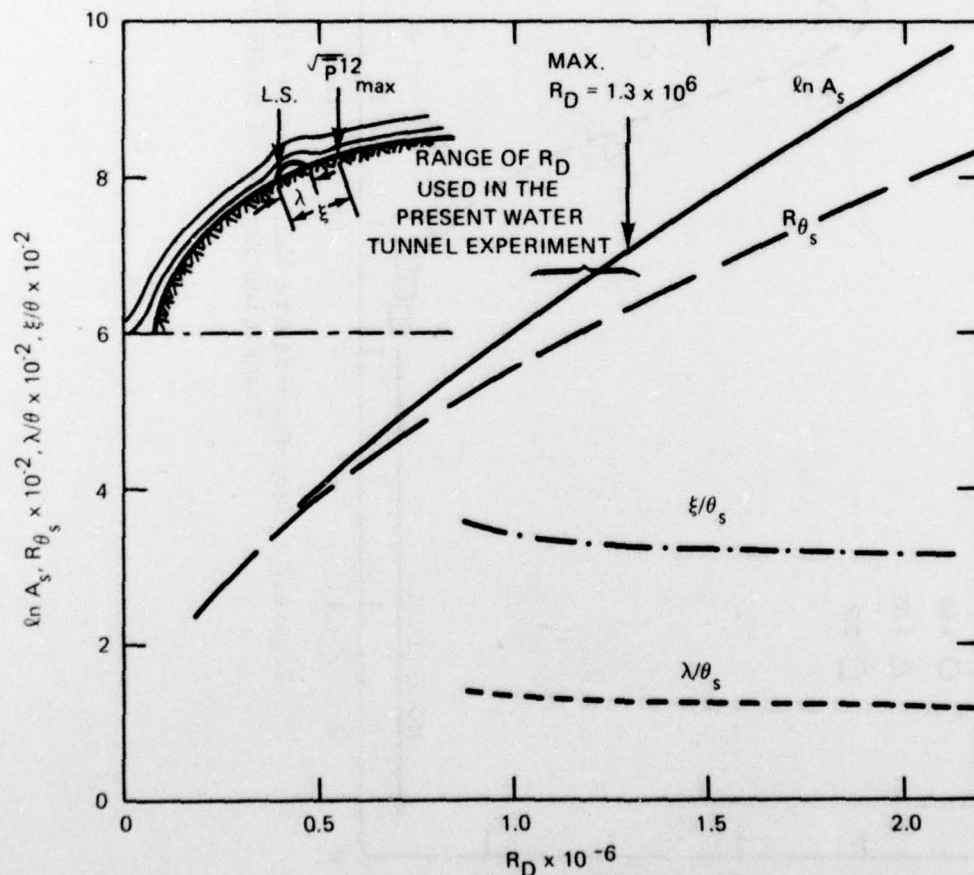Figure 3 – Surface Profile and Pressure Coefficient on Headform S-2

Figure 4 – Characteristic Parameters of Laminar Separation
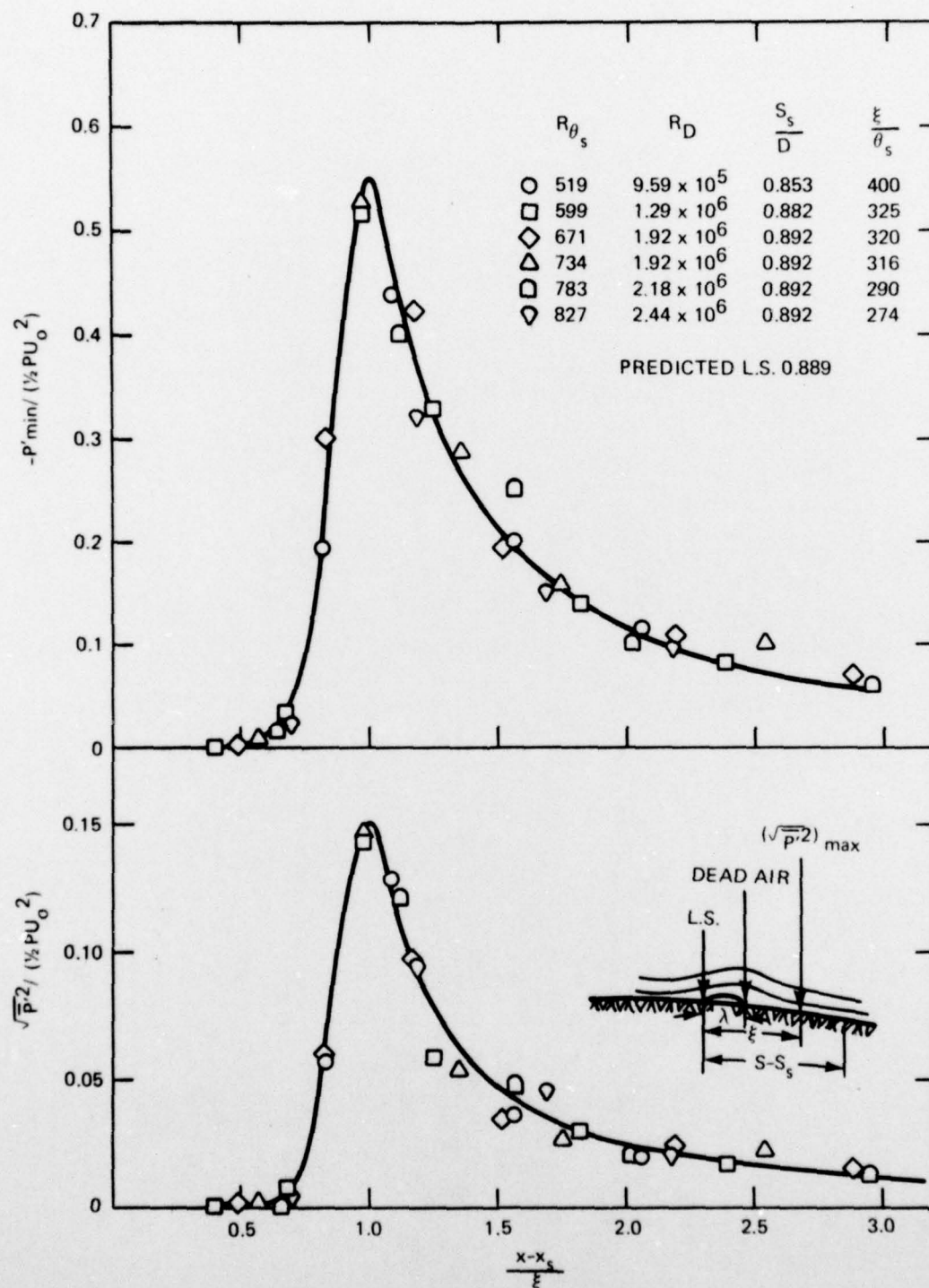on Headform S-2

0.7

0.6

R_{θ_s}	R_D	$\dfrac{S_s}{D}$	$\dfrac{\xi}{\theta_s}$
○ 519	9.59×10^5	0.853	400
□ 599	1.29×10^6	0.882	325
◇ 671	1.92×10^6	0.892	320
△ 734	1.92×10^6	0.892	316
⬠ 783	2.18×10^6	0.892	290
▽ 827	2.44×10^6	0.892	274

PREDICTED L.S. 0.889

0.5

0.4

$-P'min / (\frac{1}{2}PU_o{}^2)$

0.3

0.2

0.1

0

0.15

$\sqrt{\overline{P'^2}} / (\frac{1}{2}PU_o{}^2)$

0.10

$(\sqrt{\overline{P'^2}})_{max}$

DEAD AIR

L.S.

λ

ξ

$S-S_s$

0.05

0

0.5 1.0 1.5 2.0 2.5 3.0

$\dfrac{x-x_s}{\xi}$

Figure 5 - Root-Mean-Square and Negative Peak Wall Pressure Fluctuation
Immediately Behind Laminar Separation of Headform S-1

27

Figure 6a – Beginning of Visible Traveling Growing Cavitation Bubbles at $1.4 < x/D < 1.7$ ($\sigma = 0.173$, 18 ppmw Air Content)

Figure 6b – More Frequent Occurence of Visible Growing Cavitation Bubbles at $1.3 < x/D < 1.7$ ($\sigma = 0.167$, 18 ppmw Air Content)

Figure 6 – Various Stages of Cavitation on Headform T-3 with Natural Transition
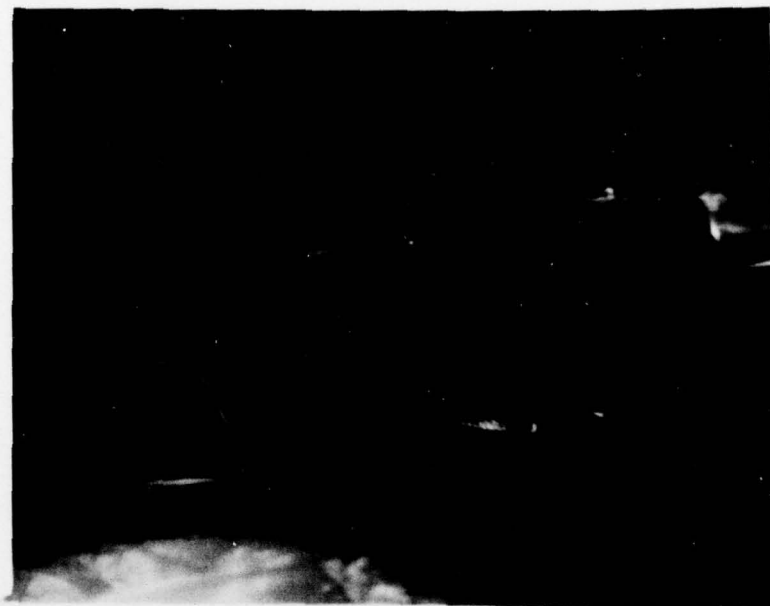
Figure 6c – In Addition to Visible Growing Bubbles, Occasional Spot Cavitation and Collapse of Cavitation Bubble at $1.7 < x/D < 2.1$ Become Visible ($\sigma = 0.157$, 18 ppmw Air Content)

Figure 6d – More Frequent Occurence of Visible Growing and Collapsing Cavitation Bubbles ($\sigma = 0.145$, 18 ppmw Air Content)

29

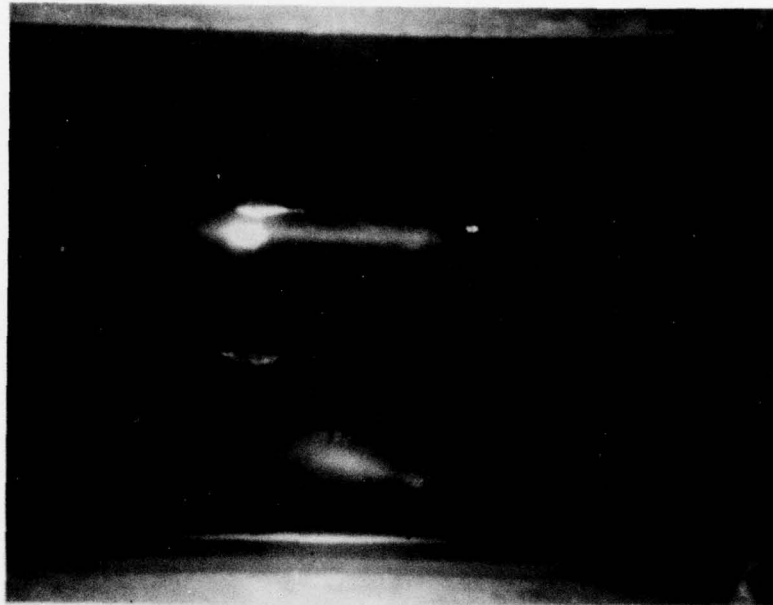Figure 6e - Intensive Cavitation (σ = 0.14, 18 ppmw Air Content)

30

Figure 7a – Formation Cavitation Finger at About the Reattachment of Laminar Separation (σ = 0.260, 9 ppmw Air Content)
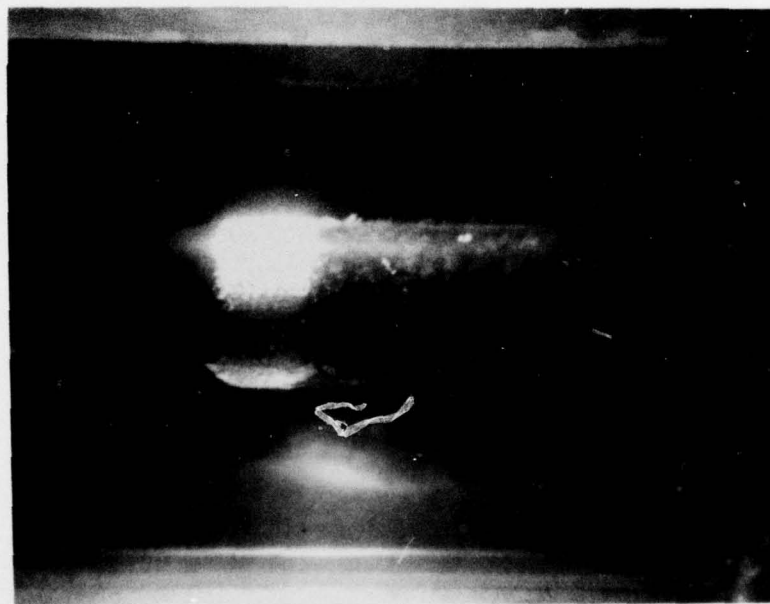

Figure 7b – Formation of Attached Ring Cavity (σ = 0.245, 9 ppmw Air Content)

Figure 7 – Various Stages of Cavitation on Headform S-2 with Laminar Separation (σ = 0.30±0.1, σ_d = 0.31±0.1, 9 ppmw Air Content)

DTNSRDC ISSUES THREE TYPES OF REPORTS

1. DTNSRDC REPORTS, A FORMAL SERIES, CONTAIN INFORMATION OF PERMANENT TECHNICAL VALUE. THEY CARRY A CONSECUTIVE NUMERICAL IDENTIFICATION REGARDLESS OF THEIR CLASSIFICATION OR THE ORIGINATING DEPARTMENT.

2. DEPARTMENTAL REPORTS, A SEMIFORMAL SERIES, CONTAIN INFORMATION OF A PRELIMINARY, TEMPORARY, OR PROPRIETARY NATURE OR OF LIMITED INTEREST OR SIGNIFICANCE. THEY CARRY A DEPARTMENTAL ALPHANUMERICAL IDENTIFICATION.

3. TECHNICAL MEMORANDA, AN INFORMAL SERIES, CONTAIN TECHNICAL DOCUMENTATION OF LIMITED USE AND INTEREST. THEY ARE PRIMARILY WORKING PAPERS INTENDED FOR INTERNAL USE. THEY CARRY AN IDENTIFYING NUMBER WHICH INDICATES THEIR TYPE AND THE NUMERICAL CODE OF THE ORIGINATING DEPARTMENT. ANY DISTRIBUTION OUTSIDE DTNSRDC MUST BE APPROVED BY THE HEAD OF THE ORIGINATING DEPARTMENT ON A CASE-BY-CASE BASIS.